

Organohalide Precursors for the Continuous Production of Photocatalytic Bismuth Oxyhalide Nanoplates

Matthew N. Gordon, Kaustav Chatterjee, Alison L. Lambright, Sandra L. A. Bueno, and Sara E. Skrabalak*

Cite This: *Inorg. Chem.* 2021, 60, 4218–4225

Read Online

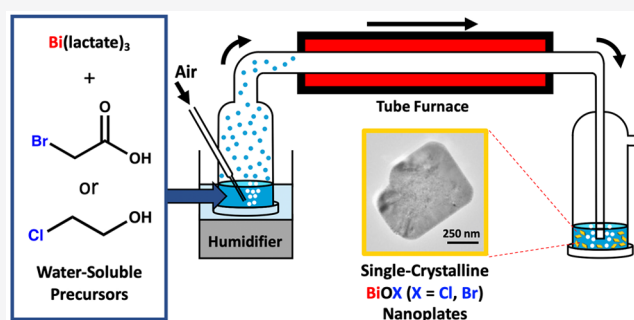
ACCESS |

Metrics & More

Article Recommendations

Supporting Information

ABSTRACT: Metal heteroanionic materials, such as oxyhalides, are promising photocatalysts in which band positions can be engineered for visible-light absorption by changing the halide identity. Advancing the synthesis of these materials, bismuth oxyhalides of the form BiOX (X = Cl, Br) have been prepared using rapid and scalable ultrasonic spray synthesis (USS). Central to this advance was the identification of small organohalide molecules as halide sources. When these precursors are spatially and temporally confined in the aerosol phase with molten salt fluxes, powders composed of single-crystalline BiOX nanoplates can be produced continuously. A mechanism highlighting the in situ generation of halide ions is proposed. These materials can be used as photocatalysts and provide proof-of-concept toward USS as a route to more complex bismuth oxyhalide materials.



INTRODUCTION

Every hour, enough solar energy reaches the surface of the Earth to meet the energy needs of the entire planet for a year.¹ This fact drives the motivation to harvest a fraction of this energy and convert it to a solar fuel. One approach is through solar water splitting wherein sunlight is used to split water into hydrogen and oxygen, a process usually mediated with a light-absorbing semiconductor.² This reaction can then be reversed upon energy demand in a hydrogen fuel cell, releasing the stored chemical energy without producing carbon-based byproducts.³ Fujishima and Honda first demonstrated water photolysis with a titanium dioxide semiconductor in 1972.⁴ Since this work, tremendous efforts have been directed toward the identification of new photocatalytic materials with improved properties and their subsequent synthesis as structurally well-defined materials.

Metal oxides typically meet the band-position requirements for water splitting but absorb only ultraviolet light because of their deep O 2p orbitals, which compose the valence band of these materials.⁵ Secondary anions that are less electronegative than oxygen can be incorporated to raise the valence-band maximum, thus reducing the overall band gap.^{6–8} Mixed-anion materials such as oxynitrides, oxysulfides, and oxyhalides (where the halide is chloride, bromide, or iodide) have been explored to combat this problem.^{9–13} For oxyhalides, the identity and composition of the halide can tune the valence-band position and band-gap energies.¹⁴

Specifically, BiOX (X = Cl, Br, and I) has a tunable band gap that decreases from BiOCl to BiOI.¹⁵ The crystal structure of

BiOX (P4/nmm, No. 129) is also advantageous to photocatalysis because of its layered Sillén structure of alternating [Bi₂O₂]²⁺ layers and X[−] double layers. These alternating charged layers create a static internal electric field perpendicular to the layers, which spatially separates charge carriers and reduces their recombination.¹⁶ BiOX materials are commonly prepared via precipitation between Bi³⁺ and halide salts. These facile syntheses are limited by the ability to control crystal growth, often resulting in materials with poorly controlled crystallinity (i.e., multiple crystalline domains in a particle). An additional postsynthetic hydrothermal treatment is often used to improve the resulting crystallinity.^{17–20} Here, both BiOCl and BiOBr powders composed of single-crystalline nanoplates with controlled faceting are achieved in a single step by ultrasonic spray synthesis (USS), a continuous-flow means of materials production.

USS is used for the commercial production of materials as fine powders; however, typically the powders consist of polycrystalline microspheres, not single-crystalline particles. This particle morphology arises from the aerosol process parameters and underlying chemistry that is typically used to produce the materials. As shown in Figure 1A, a precursor

Special Issue: Inorganic Chemistry of Nanoparticles

Received: October 31, 2020

Published: December 27, 2020



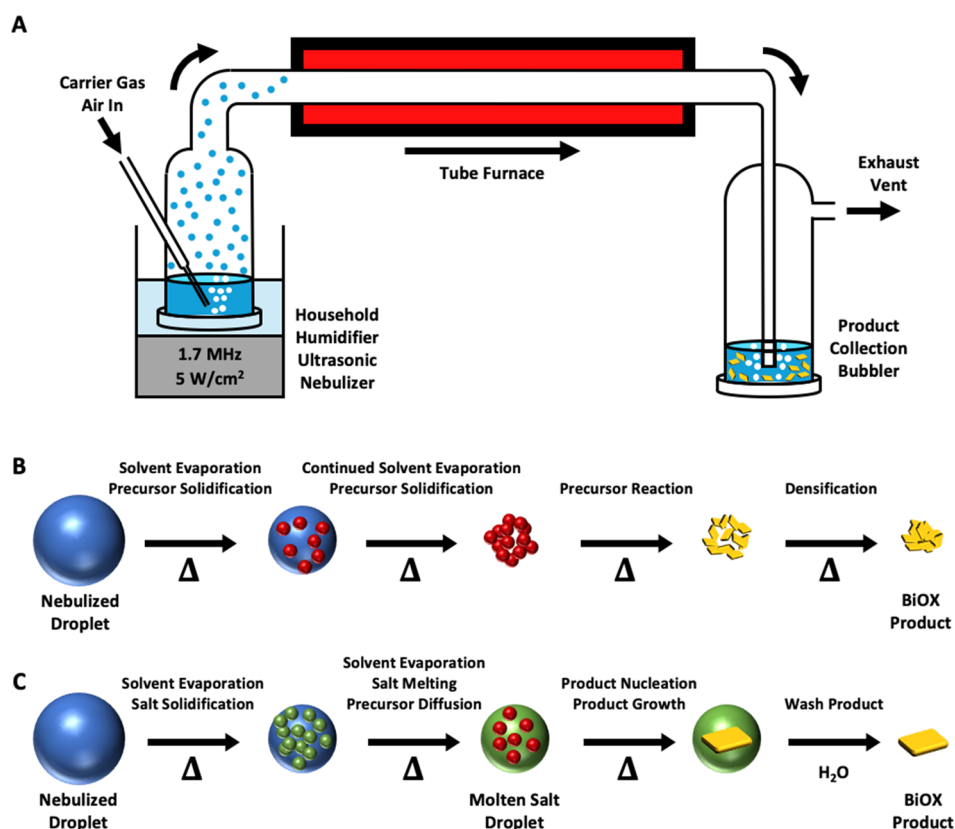


Figure 1. (A) Schematic of a USS reactor consisting of a nebulization chamber, hot wall reactor, and collection vessel. Schemes highlighting the processes that occur during USS within the droplet during heating (B) without a salt flux and (C) with a salt flux, where blue, red, green, and yellow represent water, precursors, salt flux, and BiOX product, respectively.

solution is nebulized into aerosol droplets, which travel via a carrier gas into a hot wall reactor where product formation occurs.²¹ Solvent evaporation, precursor solidification and reaction, and finally densification occur within the individual droplets, with the solid particles being collected outside of the hot wall reactor (in our setup, particles are collected in water; Figure 1B). Typically, water-soluble precursors are selected and decompose or react in a manner that produces only the desired product and volatile byproducts that are easily flushed from the droplets. Because of these chemical and physical processes, multiple crystals form within a droplet and give rise to the polycrystalline nature of product particles, where the droplet sizes are governed by the Lang equation.²²

Even so, we have shown that the temporal and spatial confinement offered by the aerosol droplets can be exploited to produce single-crystalline nanoscale crystals with shape control by incorporating an inorganic salt into precursor solutions, which becomes a molten flux upon heating in the reactor.²³ In such aerosol-assisted molten salt syntheses, the inorganic salt serves as a high-temperature solvent, which facilitates faster diffusion rates compared to solid-state reactions, and the flux itself can inhibit particle–particle fusion within individual droplets (Figure 1C).^{9,21,23–27} The latter point is central to achieving discrete, single-crystalline particles as reported here.

Ideal reagents for USS are those that are water-soluble, which then react at high temperature in the droplet to form an insoluble product. Considering the synthesis of BiOX, water-soluble bismuth precursors are rare, with common bismuth salts hydrolyzing readily in water to produce insoluble products.²⁸ Polydentate hydroxycarboxylic or aminocarboxylic

acids can complex to Bi³⁺ to produce water-soluble compounds.^{29,30} Simple halide salts would be the obvious choice as halide precursors; however, these reagents immediately replace the ligands complexing to bismuth, resulting in the uncontrolled precipitation of BiOX. Because BiOX formation should occur in the droplet phase within the hot wall reactor, a novel halide source is required.

Herein, small organohalides are shown to be effective water-soluble halide sources that are compatible with a bismuth lactate complex [denoted as Bi(lac)₃], facilitating the formation of single-crystalline BiOCl and BiOBr nanoplates when used with the aerosol-assisted molten salt synthesis approach. The mechanism of BiOX formation in the USS system is found to be nucleophilic substitution of the organohalide with water, releasing the halide to immediately precipitate with Bi(lac)₃. The reaction is temperature-controlled such that product formation only occurs in the heated droplets. USS-derived BiOCl and BiOBr were also found to be capable photocatalysts, with this work opening up a new synthetic path toward more complex bismuth-containing oxyhalides given the versatility of USS.

EXPERIMENTAL SECTION

Materials. Bismuth nitrate pentahydrate (98%), bromoacetic acid (98+%), 2-chloroethanol (99%), and 1,10-phenanthroline (anhydrous, 99%) were purchased from Alfa Aesar. Silver nitrate (≥99.0%), iron(III) nitrate nonahydrate (≥99.95% metals basis), iron(III) chloride hexahydrate (≥98%), potassium bromide (≥99%), and D₂O (99.9 atom % D) were obtained from Sigma-Aldrich. L-(+)-Lactic acid (90% solution in water) was purchased from ACROS Organics. Potassium nitrate (≥99.0%) was obtained from EMD. Potassium

chloride (ACS grade) was purchased from BDH. Methanol (AR/ACS grade), sulfuric acid (95.0–98.0%), and ethylene glycol ($\geq 99.0\%$) were obtained from Macron Fine Chemicals. Potassium oxalate monohydrate (ACS grade) and sodium acetate (anhydrous, ACS grade) were purchased from J.T. Baker. Glycolic acid (98%) was obtained from Oakwood Chemicals. Ethanol (200 proof, ACS/USP grade) was purchased from Pharmco. Tetraammineplatinum(II) chloride monohydrate (99%, 99.99% platinum) was obtained from Strem Chemicals. All chemicals were used as received. Milli-Q (18.2 M Ω -cm at 25 °C) purified water was used for all experiments, except where D₂O is noted.

Synthesis of Bi(lac)₃. The bismuth lactate precursor Bi(lac)₃ was inspired by a literature synthesis.³¹ Bismuth nitrate pentahydrate (8.73 g, 18.0 mmol, 1.00 equiv) and water (32 mL) were sonicated and stirred, forming a white precipitate. L-(+)-Lactic acid (4.43 mL, 54.0 mmol, 3.00 equiv) was added, and the mixture was stirred overnight, forming a clear Bi(lac)₃ solution. The concentration of the solution was calculated using the mass of Bi(NO₃)₃·5H₂O used and the final volume of the solution (typically ~ 0.45 M). Note that the exact structure of the Bi(lac)₃ complex is not known in solution, but because of the prevention of bismuth hydroxide precipitation, it is likely that lactate stabilizes the Bi³⁺ ion because of its bidentate ligation.³¹

USS of BiOBr Nanoplates. Figure 1A highlights the major components of the USS system, while full details of the apparatus can be found in a previous publication.²¹ In a typical BiOBr synthesis, Bi(lac)₃ (2.00 mmol, solution from above, 1.00 equiv), bromoacetic acid (360 μ L, 5.00 mmol, 2.50 equiv), and KNO₃ (2.02 g, 20.0 mmol, 10.0 equiv) are added to water, mixed, and diluted to a final volume of 20 mL. This precursor solution is transferred to the USS nebulization chamber. Air is sparged into the solution at a flow rate of ~ 175 sccm, and the furnace is set to 584 °C (250 °C above the melting point of KNO₃). After the furnace is equilibrated and the solution is sparged for more than 10 min, the nebulizer is turned on to full power (1.7 MHz, ~ 5 W/cm²). At this frequency, the number-median droplet size is estimated to be ~ 3 μ m in diameter, according to the Lang equation, and $\sim 90\%$ of the droplets are smaller than twice this value.²² Nebulized droplets are carried with the air flow through the hot wall reactor. The flow is left undisturbed overnight or until a sufficient amount of product is produced. The product is collected by bubbling the flow output from the furnace into water contained in a gas washing bottle. The solution containing product is transferred to a centrifuge tube, where it is centrifuged to separate the powder from the supernatant. The supernatant is discarded and the powder dispersed in water and then collected again by centrifugation; this washing step is conducted three times before the powder is dried under vacuum. We note that product is lost to the reactor walls and through the collection apparatus, and reactions are stopped before all of the precursor solution is nebulized. Even with these losses, our yields are $\sim 20\%$ at a nebulization rate of ~ 2 mL/h, which provides 100–200 mg/day. Commercial reactors are quite different in design and can produce on the kilogram scale with minimal losses.²³

USS of BiOCl Nanoplates. BiOCl is produced in a manner similar to that above for BiOBr using 2-chloroethanol (335 μ L, 5.00 mmol, 2.50 equiv) instead of bromoacetic acid and a furnace temperature of 484 °C (150 °C above the melting point of KNO₃).

Ex Situ Mechanism Studies. Experiments to probe the mechanism by NMR were conducted using a solution analogous to the nebulization mixture. A round-bottomed flask equipped with a stir bar was charged with an organohalide (2.50 mmol, 1.00 equiv, bromoacetic acid or 2-chloroethanol), silver nitrate (0.42 g, 2.5 mmol, 1.0 equiv), and D₂O (10 mL). The flask was sparged with air and equipped with a water condenser. The reaction was heated in an oil bath at 100 °C. Aliquots (1 mL) were removed at specific time points and analyzed by ¹H NMR.

Synthesis of Bulk BiOX. For a comparison to USS samples, bulk BiOBr and BiOCl samples were also synthesized by standard precipitation routes from the literature.²⁰ Bismuth nitrate pentahydrate (4.85 g, 10.0 mmol, 1.00 equiv) was dissolved in ethanol (50 mL), which forms a white suspension. Separately, KBr (1.19 g, 10.0

mmol, 1.00 equiv) was dissolved in water (20 mL). The KBr solution was added dropwise to the bismuth mixture with stirring. The mixture was stirred for 5 h, and then the solid BiOX was collected via filtration. Last, the product was washed three times with ethanol and water and dried under vacuum. Bulk BiOCl was made similarly using KCl (0.75 g, 10 mmol, 1.0 equiv) in place of KBr. These bulk samples were compared to the USS BiOX samples in photocatalytic experiments.

Electron Microscopy. Scanning electron microscopy (SEM) was performed using a FEI Quanta 600 FEG microscope, operating at 30 kV with a spot size of 3, that interfaces with an Oxford INCA detector for energy-dispersive X-ray spectroscopy (EDS) analysis. Samples for SEM imaging were prepared by dispersing the particles in water with sonication, followed by drop-casting 2 μ L of the solution onto a silicon wafer that was allowed to dry while loosely covered. High-resolution transmission electron microscopy (TEM) images, scanning transmission electron microscopy (STEM) images, and selected-area electron diffraction (SAED) patterns were collected on a JEOL JEM 3200FS microscope operating at 300 kV using a Gatan 4K \times 4K Ultrascan 4000 camera. The instrument interfaces with an Oxford INCA detector for EDS mapping. Samples for TEM/STEM analysis were prepared by drop-casting 3 μ L of a dispersed aqueous particle solution onto a 300-mesh carbon-coated copper grid and allowed to dry while loosely covered.

Powder X-ray Diffraction (pXRD). pXRD data was collected with a PANalytical Empyrean instrument equipped with Cu K α radiation (1.54178 Å) and an X'Celerator linear strip detector. An accelerating voltage of 45 kV and 40 mA current was used for all measurements. Scanning was from 5 to 80° 2-theta, with a step size of 0.0167° 2-theta. Powders were measured on a zero-background rotating silicon holder.

NMR Spectroscopy. ¹H NMR spectra were recorded at room temperature on a Varian I400 (400 MHz) or Varian VXR400 (400 MHz) spectrometer. Chemical shifts are reported in parts per million from tetramethylsilane, with the residual solvent resonance as the internal standard (D₂O: δ = 4.79 ppm).

Optical Properties. Diffuse-reflectance spectroscopy (DRS) was conducted on a Cary 100 UV–visible spectrophotometer equipped with a Cary 301 diffuse-reflectance accessory using BaSO₄ powder as a reference.

X-ray Photoelectron Spectroscopy (XPS). XPS measurements were collected using a PHI 5000 Versa Probe II scanning X-ray microprobe under ultrahigh-vacuum conditions with a monochromatic Al K α X-ray source. Spectra were shifted based on the C 1s peak (284.8 eV) of adventitious carbon.

Photocatalytic Testing. Photocatalytic testing was performed in a 25 mL quartz reactor connected to a gas closed-circulation system with side irradiation by a xenon lamp (Newport 66902, 300 W) attached with a water filter to avoid near-IR radiation above 850 nm (Figure S1). The power density on the reactor was found to be 743 mW/cm² (full arc) using a power meter (Newport 1917-R, 818P-040-25 sensor). The rate of incident photons was calculated as 7.42×10^{17} photons/s (corresponding to 36.8 mW/mL) by ferrioxalate actinometry for $\lambda < 500$ nm (details can be found in the Supporting Information). For oxygen evolution reaction (OER) tests, BiOX powder (10 mg) was dispersed in the quartz reactor in aqueous Fe(NO₃)₃ [5 mM, 10 mL, previously adjusted to pH 2.4 with HNO₃ to prevent Fe(OH)₃ precipitation]. For hydrogen evolution reaction (HER) experiments, BiOX was first loaded with 1 wt % platinum based on a literature method.²⁶ BiOX powder was impregnated in a [Pt(NH₃)₄]Cl₂ solution, followed by annealing at 300 °C for 1 h under forming gas (5% H₂ in N₂). Pt/BiOX powder (10 mg) was dispersed in an aqueous solution containing methanol (10 vol %, 10 mL). For both the OER and HER experiments, the chamber was evacuated under vacuum followed by backfilling of the system to atmospheric pressure with helium (for OER experiments) or argon (for HER experiments) three times. The headspace gas concentration was monitored over the course of 4 h of irradiation with stirring. A total of 0.5 mL of headspace gas was manually withdrawn using a gastight syringe and injected into a gas chromatograph interfaced with

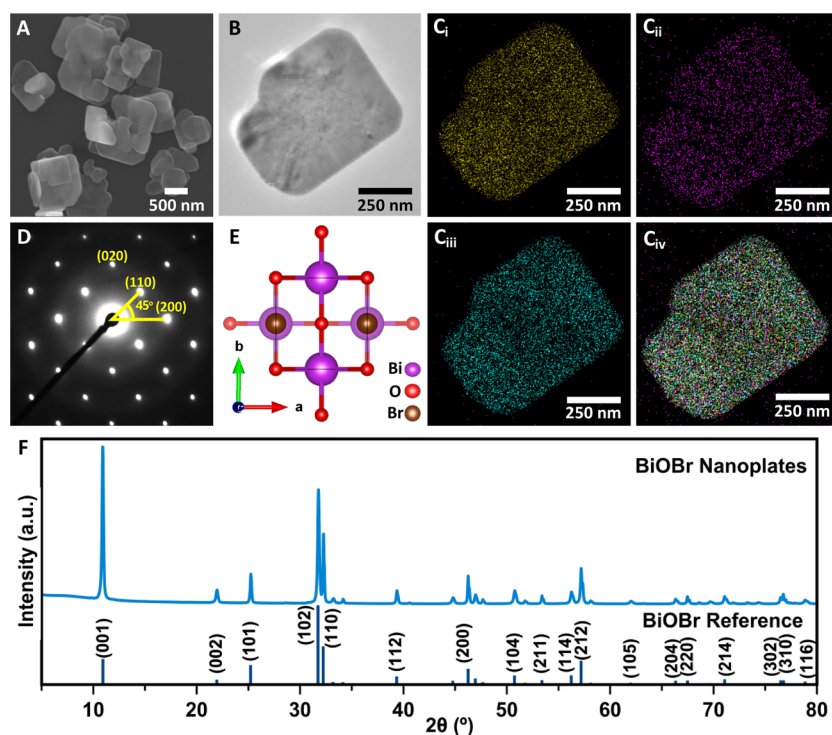


Figure 2. (A) SEM image of BiOBr nanoplates. (B) TEM image of a BiOBr nanoplate. (C) STEM–EDS elemental mapping of part B showing the presence of (C_i) bismuth (yellow), (C_{ii}) oxygen (magenta), (C_{iii}) bromine (cyan), and (C_{iv}) combined bismuth, oxygen, and bromine signals. (D) SAED pattern of part B with reflections indexed. (E) Depiction of the BiOBr crystal structure ($P4/nmm$, No. 129) viewed along the $[001]$ direction. (F) pXRD pattern of BiOBr with a reference pattern (JCPDS 73-2061).

a thermal conductivity detector (Agilent Technologies 6890N gas chromatograph, molecular sieve, MS6E column). Nitrogen was used as an internal standard to approximate the introduction of dioxygen from air during manual injection of the sample to the gas chromatograph for OER measurements.

pH. The pH was measured with a VWR sympHony pH meter calibrated before use using standard buffer solutions.

RESULTS AND DISCUSSION

Both BiOBr and BiOCl have been achieved as powders composed of discrete, single-crystalline nanoplates through the judicious selection of precursors for aerosol-assisted molten salt synthesis. Shown in Figure 2 is the characterization of BiOBr nanoplates produced in this manner. They were achieved by nebulizing an aqueous solution containing KNO_3 as a flux, bromoacetic acid as a Br^- source, and $\text{Bi}(\text{lac})_3$ as a Bi^{3+} source. Although a number of fluxes and reaction temperatures were surveyed, as discussed later, the highest quality samples in terms of phase purity and nanocrystal form were obtained with KNO_3 at a reactor temperature of $584\text{ }^\circ\text{C}$ [$250\text{ }^\circ\text{C}$ above the melting point of KNO_3]. SEM (Figures 2A and S2) and TEM (Figure 2B) show nanoplates that are roughly 300–1000 nm in length and width, with thicknesses of about 30–80 nm. STEM-EDS elemental mapping shows spatially homogeneous signals from bismuth, oxygen, and bromine, consistent with a uniform composition throughout individual particles (Figure 2C_{i–iv}). The bulk elemental ratio of Bi/Br is 1.07 by SEM–EDS, indicating a slightly halogen-deficient sample. A single set of diffraction spots in the SAED pattern (Figure 2D) indicates that individual nanoplates are single-crystalline. The SAED pattern corresponds to the nanoplate being viewed down the $[001]$ zone axis, oriented as shown in the included crystal

structure (Figure 2E). pXRD of the product shows BiOBr as the only crystalline product (Figure 2F). Additionally, the pXRD pattern shows a much higher relative signal for the (001) reflection compared to the reference, further highlighting the exposed $\{001\}$ facets and preferred orientation of the nanoplates.

Similar results were achieved for the synthesis of BiOCl nanoplates, but now with 2-chloroethanol as a Cl^- source (Figure S3). Again, optimized results were obtained with KNO_3 as the droplet flux but at a lower furnace temperature of $484\text{ }^\circ\text{C}$ ($150\text{ }^\circ\text{C}$ above the melting point of KNO_3). SEM and TEM images show nanoplates that are confirmed to be single-crystalline by SAED (Figure S3A,B,D,E). They have a homogeneous elemental distribution by STEM–EDS (Figure S3C_{i–iv}). The pXRD pattern confirms BiOCl as the only crystalline phase (Figure S3F).

Other organohalide molecules were screened, including 2-bromoethanol and chloroacetic acid as well as 2-bromoethyl methyl ether, 2-bromopropionic acid, 2,2-dichloroethanol, epichlorohydrin, and ethyl chloroacetate. All produced the respective BiOX phase, although some had impurity phases (such as Bi_2O_3) and less ideal particle morphologies. Ultimately, bromoacetic acid and 2-chloroethanol were chosen for further study because of their high water solubility and the quality of the resulting BiOX samples in terms of phase purity and plate morphology.

Two synthetic parameters were found to be most critical to the formation of single-crystalline nanoplates: precursor selection and integration of a suitable flux into USS. Although the high reaction temperatures and short droplet residence times can limit analyses of the chemistry occurring during USS, we undertook a detailed mechanistic study that accounts for BiOX nanoplate formation. This work establishes organo-

halides as a general source of halide ions that should be applicable to other oxyhalide materials, even beyond USS syntheses (e.g., hydrothermal routes). This is in complement to work by Rabuffetti and co-workers that demonstrated metal trifluoroacetates as precursor complexes toward layered perovskite systems where the fluorinated ligand provides the necessary F^- for the reactions.^{32–34} In aqueous solution, Bi^{3+} and X^- react quickly to form $BiOX$ as a precipitate except at extremely low pH values. With this in mind, we hypothesized that Br^- and Cl^- were being generated from the organohalides at elevated temperatures within the droplets via nucleophilic substitution, with water acting as a nucleophile.^{35–39}

While in situ experiments are not possible, ex situ experiments were performed to mimic the reaction and test this hypothesis. In the case of Br^- generation, a solution of bromoacetic acid, silver nitrate, and D_2O was heated and monitored using 1H NMR (Figure 3). $AgNO_3$ was selected as

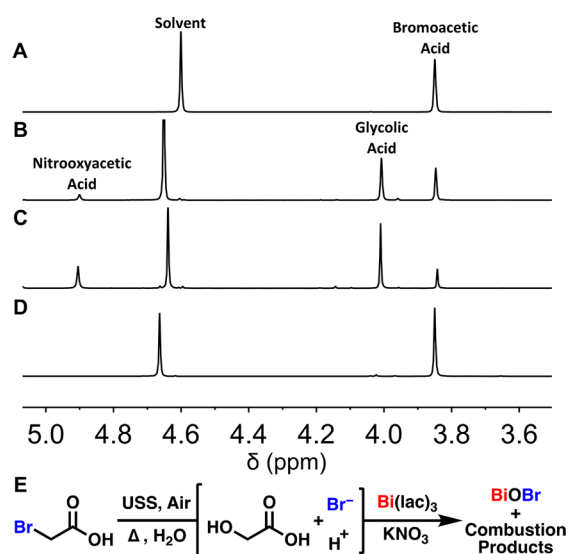


Figure 3. 1H NMR of bromoacetic acid and $AgNO_3$ in D_2O (A) without heating, (B) after heating at $100\text{ }^\circ\text{C}$ for 45 min, (C) after heating at $100\text{ }^\circ\text{C}$ for 90 min, and (D) after heating at $100\text{ }^\circ\text{C}$ for 90 min while omitting $AgNO_3$, (E) Proposed $BiOBr$ production scheme.

a scavenger of Br^- instead of $Bi(lac)_3$ in order to simplify the NMR spectra, with $AgBr(s)$ readily precipitating out with any free Br^- , just as $BiOBr(s)$ forms when Bi^{3+} is exposed to free Br^- . Before heating, 1H NMR of this solution shows one singlet peak at 3.85 ppm from the bromoacetic acid starting material, indicating that no reaction occurs at room temperature (Figure 3A). Additionally, no solid precipitate is produced. Upon heating at $100\text{ }^\circ\text{C}$ for 45 min, a new major singlet peak appears at 4.0 ppm, corresponding to glycolic acid, the product of a substitution reaction replacing the bromide group with a hydroxyl group from water (Figure 3B). A minor singlet peak at 4.9 ppm is visible as well, identified as nitrooxyacetic acid, the substitution product of nitrate replacing bromide (Figure S4).⁴⁰ A solid precipitate is observed as well, identified as $AgBr$ by pXRD (Figure S5). Upon further heating at $100\text{ }^\circ\text{C}$ for 90 min total, the relative size of the peak from the bromoacetic acid starting material further decreases, while the peaks from both major and minor products increase, showing further progression in the reaction (Figure 3C). A control experiment without $AgNO_3$ shows no glycolic acid production or precipitation despite heating at 100

$^\circ\text{C}$ for 90 min (Figure 3D), highlighting the need for a reagent to remove halides from the reaction as they form. Applying this mechanistic insight to the USS system, the $Bi(lac)_3$ reagent serves the same role as $AgNO_3$ to precipitate any autogenous halide ions as $BiOX$, our desired product (Figure 3E).

Analogous experiments were performed to verify the Cl^- release from 2-chloroethanol. The ex situ reaction scheme shows a similar substitution reaction from heating 2-chloroethanol with $AgNO_3$ in D_2O to produce ethylene glycol and $AgCl$ as major products and 2-nitrooxyethanol as a minor product (Figure S6). Before heating, this solution shows two triplet peaks centered at 3.55 and 3.7 ppm from 2-chloroethanol, indicating that no reaction occurs at room temperature (Figure S6A). Upon heating at $100\text{ }^\circ\text{C}$ for 90 min, a new major singlet peak appears at 3.5 ppm, which corresponds to ethylene glycol, the product of a substitution reaction of water displacing chloride (Figure S6B; note that the peak is a singlet due to the symmetry of ethylene glycol). Two minor triplet peaks centered at 3.75 and 4.5 ppm were just visible as well, which correspond to 2-nitrooxyethanol, the substitution product of chloride being replaced with a nitrate group. Upon further heating at $100\text{ }^\circ\text{C}$ for 6 h total, the peak from the 2-chloroethanol starting material is gone, while the peaks from both the major and minor products increase, showing completion of the reaction (Figure S6C). The identity of the minor product, 2-nitrooxyethanol, was confirmed through a known synthesis and by comparison of the spectra (Figure S6D).⁴¹ Similar to the mechanism for $BiOBr$ production, a nucleophilic substitution mechanism is proposed to form the $BiOCl$ products in the USS system (Figure S6E).

These ex situ results highlight the importance of each component of the synthesis. $Bi(lac)_3$ serves as a water-soluble source of bismuth for $BiOX$ but also as a necessary tool to capture the released halide ions as they form. The organohalide reagents (bromoacetic acid and 2-chloroethanol) serve as halide sources but in a unique manner, such that they react with water only at elevated temperatures. This property makes the solution stable at room temperature and capable of nebulization into aerosol droplets for transport into the USS reactor, where the reactions occur to facilitate product formation. While the ex situ experiments could only be conducted at $100\text{ }^\circ\text{C}$, these reactions would proceed much more quickly at the elevated temperatures of the droplets.

While the ex situ mechanistic experiments give insight into the chemistry occurring within the aerosol droplets to form $BiOX$, they do not account for the morphology of the $BiOX$ particles. The aerosol approach coupled with KNO_3 as a flux is central to achieving single-crystalline nanoplates of $BiOBr$ and $BiOCl$ with facet control. Specifically, when an otherwise identical USS experiment is conducted without the flux, powders composed of polycrystalline, hollow spheres in the case of $BiOCl$ and hard aggregates of nanoplates in the case of $BiOBr$ are produced (Figure S7). The pXRD patterns of the products show $BiOX$ without other crystalline phases. However, the product morphologies are undesired for photocatalytic applications because polycrystalline materials suffer from a high recombination of charge carriers and large aggregates have limited active sites.^{42,43} These morphologies are characteristic of those prepared by traditional USS because multiple crystallites form per droplet and aggregate together as the liquid evaporates.⁴⁴ These results also highlight the importance of flux addition in achieving single-crystalline particles with facet control.

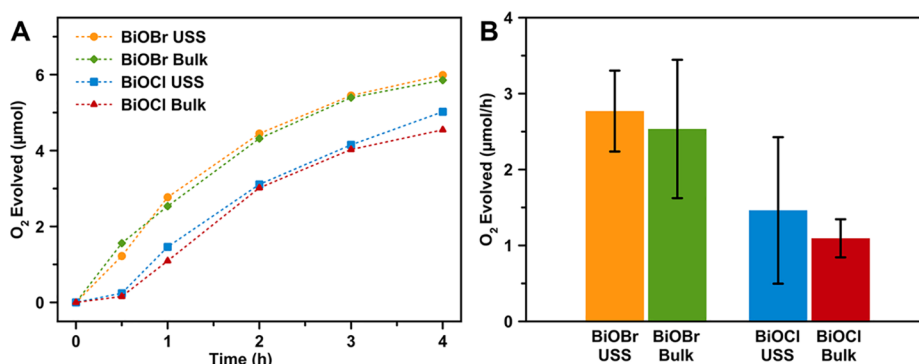


Figure 4. (A) Time courses of photocatalytic OER on the BiOX USS samples compared to BiOX synthesized by bulk precipitation. (B) Oxygen evolution rate for these samples after 1 h. The graph shows the average of a minimum of three experiments with standard deviations. The graph in part A has its standard deviations removed for clarity but can be found in Figure S13C. Reaction conditions: OER, 10 mg sample in 10 mL of 5 mM Fe(NO₃)₃ (previously adjusted to pH 2.4 with HNO₃ to prevent Fe(OH)₃ precipitation), 300 W xenon lamp (full arc).

Even though flux addition is important in achieving single-crystalline particles, not all fluxes studied facilitated the production of single-crystalline BiOX nanoplates or were compatible with the precursors. For example, Bi(lac)₃ reacts to produce a precipitate in the presence of halide salts and other strongly π -donating anions. Nitrate salts were soluble with Bi(lac)₃ and have low melting points, which makes them ideal for USS. Among the alkali and alkali-earth nitrates, KNO₃ did not give rise to impurities/competing phases. The use of KNO₃ also led to the best product morphology. A KNO₃/Bi(lac)₃ ratio of 10:1 was found to be optimal, although slight changes were tolerable, giving rise to discrete and well-developed nanoplates.

The particle morphology was also influenced by the reactor temperature. For the case of BiOCl, the powder produced at 484 °C consisted of single-crystalline nanoplates, while higher temperatures gave a powder of microspheres comprised of many nanoplates (Figure S8). These differences in morphology can be rationalized in terms of droplet supersaturation. Specifically, fewer nucleation events occur per droplet at lower temperatures (i.e., slower reaction rates keep supersaturation low), resulting in single-crystalline plates separated by the flux.²³ In contrast, higher temperatures give a faster reaction rate and higher supersaturation; this condition provides more nucleation events and growing nanoplates per droplet.⁴⁴ Thus, the flux cannot adequately inhibit aggregation of the many particles produced, and polycrystalline microspheres are produced. This important role of KNO₃ is further supported by analysis of the BiOBr product collected prior to the gas washing bottle. Together, SEM and pXRD reveal multiple BiOBr nanoplates encased in each solidified KNO₃ microsphere (Figure S9A,C); washing the sample with water (as would occur as the droplets enter the gas washing bottle) dissolves the KNO₃ and releases the individual BiOBr nanoplates (Figure S9B,C).

With the mechanisms accounting for nanoplate formation better understood, the highest-quality BiOBr and BiOCl nanoplates (Figures 2 and S3, respectively) were characterized further, including for their photocatalytic capabilities. DRS spectra and Tauc plots of the BiOBr and BiOCl nanoplates indicate indirect band gaps of 2.83 and 3.38 eV, respectively (Figure S10), which are comparable to the reported values.⁴⁵ XPS was used to probe the surface chemical states of the nanoplate samples. The survey scans did not detect any of the unique elements from the KNO₃ flux (Figure S11A). High-

resolution scans of the bismuth, oxygen, chlorine, and bromine regions show characteristic peaks that match literature values (Figure S11B–E).⁴⁶ While elemental analysis by SEM–EDS (bulk measurement) only revealed slight halide deficiencies, XPS (surface-sensitive measurement) found much greater halide deficiencies (Table S1). This finding may be significant to the use of these materials as photocatalysts because the band structure may be different at the surface where reactions occur.

Both of the BiOBr and BiOCl nanoplates were evaluated as photocatalysts for the OER and HER half-reactions that compose the overall water splitting and compared to the BiOBr and BiOCl references prepared by bulk precipitation.²⁰ Characterization of the reference materials by SEM and pXRD can be seen in Figure S12. Water oxidation (OER) experiments show comparable activity between USS-synthesized BiOX samples and their respective bulk counterparts (Figure 4). BiOBr samples show higher evolution of oxygen than BiOCl because of their smaller band gaps and thus greater light absorbance.⁴⁷ Oxygen production continued throughout the 4 h experiments, with some decrease in the evolution rate over time (Figure 4A and S13C). The deviation from linearity is likely a result of some photocorrosion of BiOX, a known limitation of these materials.⁴⁶ Future work aims to develop more complex bismuth oxyhalide materials without this limitation. The oxygen evolution rate after 1 h is shown in Figure 4B, and USS samples show slight improvements over the bulk counterparts (although within the standard deviation of the measurements). Such an improvement could be a result of the improved crystallinity (single crystallinity vs polycrystallinity), which would lead to fewer defect sites and thus less recombination.¹⁵

In analogous water reduction (HER) experiments of BiOX USS and bulk samples, hydrogen production was not detected by our analytical system without a cocatalyst. However, platinum has been shown to be an ideal surface for HER reactions, so 1 wt % was loaded on the materials.⁴⁸ In this case, excited electrons in BiOX migrate to the platinum surfaces, where HER occurs. Figures S14 and S15 show characterization after platinum loading of the USS and bulk BiOX materials, respectively. The Pt/BiOBr sample shows higher evolution of hydrogen than Pt/BiOCl because of its smaller band gap and thus greater light absorbance (Figure S13). Hydrogen production increased over the full 4 h of measurement, with some increase in the rate of gas evolution over time (Figure S13A). The increase in the rate is thought to be a result of

some reduction of Bi^{3+} to $\text{Bi}(s)$, which may lead to enhanced light absorbance due to the surface plasmon resonance and cocatalytic properties of bismuth.^{46,49} The hydrogen evolution rate after 1 h is shown in Figure S13B, and Pt/BiOBr by USS clearly outperforms the bulk Pt/BiOBr sample. For Pt/BiOCl, the comparison between the USS and bulk samples is much closer; however, the USS sample has somewhat higher activity over the bulk counterpart. Through these studies, we show that single-crystalline BiOX nanoplates synthesized by USS match or slightly outperform their bulk counterparts, demonstrating their efficacy as photocatalysts for water splitting. These materials have other applications in CO_2 reduction and nitrogen fixation and as films for photoelectrochemical water splitting, which may be explored further.^{46,50,51}

In summary, USS was shown as a continuous route toward BiOX materials. Central to this demonstration was the identification of organohalides as a new halide source, being water-soluble and forming stable solutions with bismuth-containing complexes. As we found, such solutions could be nebulized and transported into the heated USS reactor, where nucleophilic substitution of the organohalides with water releases the halide to immediately precipitate with the bismuth complexes. Alkali nitrate salts can also be added to these solutions to establish a molten flux within the aerosol droplets that facilitates BiOX nanoplate formation in contrast to BiOX of the ill-defined morphology. We anticipate that more complex oxyhalide materials as well as perovskite halide materials can be prepared with these organohalides as a source of halide. An attractive feature of these organohalides is that their reactivity is temperature-controlled, making them well suited for USS but also by hydrothermal strategies toward new materials.

■ ASSOCIATED CONTENT

SI Supporting Information

The Supporting Information is available free of charge at <https://pubs.acs.org/doi/10.1021/acs.inorgchem.0c03231>.

BiOCl characterization, ^1H NMR of the BiOCl mechanism study, additional materials characterization, results from control experiments, actinometry details, and NMR data (PDF)

■ AUTHOR INFORMATION

Corresponding Author

Sara E. Skrabalak – Department of Chemistry, Indiana University - Bloomington, Bloomington, Indiana 47405, United States; orcid.org/0000-0002-1873-100X;
Email: sskrabal@indiana.edu

Authors

Matthew N. Gordon – Department of Chemistry, Indiana University - Bloomington, Bloomington, Indiana 47405, United States; orcid.org/0000-0001-7212-9047

Kaustav Chatterjee – Department of Chemistry, Indiana University - Bloomington, Bloomington, Indiana 47405, United States; orcid.org/0000-0003-3527-9796

Alison L. Lambright – Department of Chemistry, Indiana University - Bloomington, Bloomington, Indiana 47405, United States

Sandra L. A. Bueno – Department of Chemistry, Indiana University - Bloomington, Bloomington, Indiana 47405, United States

Complete contact information is available at:
<https://pubs.acs.org/doi/10.1021/acs.inorgchem.0c03231>

Author Contributions

The manuscript was written through contributions of all authors. All authors have given approval to the final version of the manuscript.

Funding

Funding for this project was made available from Indiana University. S.L.A.B. was supported by National Science Foundation (NSF) Grant DGE-1342962 (Graduate Research Fellowship Program). Access to the powder diffractometer was provided by NSF Grant CRIF CHE-1048613 and to the XPS by NSF Grant DMR MRI 1126394.

Notes

The authors declare no competing financial interest.

■ ACKNOWLEDGMENTS

We thank the IU Electron Microscopy Center, Molecular Structure Center, Nanoscale Characterization Facility, and Nuclear Magnetic Resonance Facility for access to the necessary instrumentation. We also thank Prof. Kevin Brown for his feedback.

■ REFERENCES

- (1) Lewis, N. S.; Crabtree, G. *Basic Research Needs for Solar Energy Utilization: Report of the Basic Energy Sciences Workshop on Solar Energy Utilization*; U.S. Department of Energy, Office of Basic Energy Science: Washington, DC, 2005.
- (2) Walter, M. G.; Warren, E. L.; McKone, J. R.; Boettcher, S. W.; Mi, Q.; Santori, E. A.; Lewis, N. S. Solar Water Splitting Cells. *Chem. Rev.* **2010**, *110*, 6446–6473.
- (3) Nocera, D. G. Solar Fuels and Solar Chemicals Industry. *Acc. Chem. Res.* **2017**, *50*, 616–619.
- (4) Fujishima, A.; Honda, K. Electrochemical Photolysis of Water at a Semiconductor Electrode. *Nature* **1972**, *238*, 37–38.
- (5) Woodhouse, M.; Parkinson, B. A. Combinatorial Approaches for the Identification and Optimization of Oxide Semiconductors for Efficient Solar Photoelectrolysis. *Chem. Soc. Rev.* **2009**, *38*, 197–210.
- (6) Cui, J.; Li, C.; Zhang, F. Development of Mixed-Anion Photocatalysts with Wide Visible-Light Absorption Bands for Solar Water Splitting. *ChemSusChem* **2019**, *12*, 1872–1888.
- (7) Maeda, K.; Domen, K. New Non-Oxide Photocatalysts Designed for Overall Water Splitting under Visible Light. *J. Phys. Chem. C* **2007**, *111*, 7851–7861.
- (8) Chun, W.-J.; Ishikawa, A.; Fujisawa, H.; Takata, T.; Kondo, J. N.; Hara, M.; Kawai, M.; Matsumoto, Y.; Domen, K. Conduction and Valence Band Positions of Ta_2O_5 , TaON, and Ta_3N_5 by UPS and Electrochemical Methods. *J. Phys. Chem. B* **2003**, *107*, 1798–1803.
- (9) Abeysinghe, D.; Skrabalak, S. E. Toward Shape-Controlled Metal Oxynitride and Nitride Particles for Solar Energy Applications. *ACS Energy Lett.* **2018**, *3*, 1331–1344.
- (10) Sun, S.; Hisatomi, T.; Wang, Q.; Chen, S.; Ma, G.; Liu, J.; Nandy, S.; Mingishi, T.; Katayama, M.; Domen, K. Efficient Redox-Mediator-Free Z-Scheme Water Splitting Employing Oxysulfide Photocatalysts under Visible Light. *ACS Catal.* **2018**, *8*, 1690–1696.
- (11) Chen, X.; Shen, S.; Guo, L.; Mao, S. S. Semiconductor-Based Photocatalytic Hydrogen Generation. *Chem. Rev.* **2010**, *110*, 6503–6570.
- (12) Wang, Q.; Nakabayashi, M.; Hisatomi, T.; Sun, S.; Akiyama, S.; Wang, Z.; Pan, Z.; Xiao, X.; Watanabe, T.; Yamada, T.; Shibata, N.; Takata, T.; Domen, K. Oxysulfide Photocatalyst for Visible-Light-Driven Overall Water Splitting. *Nat. Mater.* **2019**, *18*, 827–832.
- (13) Xiao, X.; Liu, C.; Hu, R.; Zuo, X.; Nan, J.; Li, L.; Wang, L. Oxygen-Rich Bismuth Oxyhalides: Generalized One-Pot Synthesis,

Band Structures and Visible-Light Photocatalytic Properties. *J. Mater. Chem.* **2012**, *22*, 22840–22843.

(14) Kato, D.; Hongo, K.; Maezono, R.; Higashi, M.; Kunioku, H.; Yabuuchi, M.; Suzuki, H.; Okajima, H.; Zhong, C.; Nakano, K.; Abe, R.; Kageyama, H. Valence Band Engineering of Layered Bismuth Oxyhalides toward Stable Visible-Light Water Splitting: Madelung Site Potential Analysis. *J. Am. Chem. Soc.* **2017**, *139*, 18725–18731.

(15) Di, J.; Xia, J.; Li, H.; Guo, S.; Dai, S. Bismuth Oxyhalide Layered Materials for Energy and Environmental Applications. *Nano Energy* **2017**, *41*, 172–192.

(16) Wang, L.; Wang, L.; Du, Y.; Xu, X.; Dou, S. X. Progress and Perspectives of Bismuth Oxyhalides in Catalytic Applications. *Mater. Today Phys.* **2021**, *16*, 100294.

(17) Zhang, X.; Wang, X. B.; Wang, L. W.; Wang, W. K.; Long, L. L.; Li, W. W.; Yu, H. Q. Synthesis of a Highly Efficient BiOCl Single-Crystal Nanodisk Photocatalyst with Exposing {001} Facets. *ACS Appl. Mater. Interfaces* **2014**, *6*, 7766–7772.

(18) Shenawi-Khalil, S.; Uvarov, V.; Kritsman, Y.; Menes, E.; Popov, I.; Sasson, Y. A New Family of BiO(Cl_xBr_{1-x}) Visible Light Sensitive Photocatalysts. *Catal. Commun.* **2011**, *12*, 1136–1141.

(19) Xiong, J.; Cheng, G.; Li, G.; Qin, F.; Chen, R. Well-Crystallized Square-Like 2D BiOCl Nanoplates: Mannitol-Assisted Hydrothermal Synthesis and Improved Visible-Light-Driven Photocatalytic Performance. *RSC Adv.* **2011**, *1*, 1542–1553.

(20) He, Y.; Zhang, Y.; Huang, H.; Tian, N.; Guo, Y.; Luo, Y. A Novel Bi-Based Oxybromide Bi₄NbO₈Br: Synthesis, Characterization and Visible-Light-Active Photocatalytic Activity. *Colloids Surf., A* **2014**, *462*, 131–136.

(21) Fu, J.; Daanen, N. N.; Rugen, E. E.; Chen, D. P.; Skrabalak, S. E. Simple Reactor for Ultrasonic Spray Synthesis of Nanostructured Materials. *Chem. Mater.* **2017**, *29*, 62–68.

(22) Lang, R. J. Ultrasonic Atomization of Liquids. *J. Acoust. Soc. Am.* **1962**, *34*, 6–8.

(23) Chen, D. P.; Fu, J.; Skrabalak, S. E. Towards Shape Control of Metal Oxide Nanocrystals in Confined Molten Media. *ChemNanoMat* **2015**, *1*, 18–26.

(24) Fu, J.; DeSantis, C. J.; Weiner, R. G.; Skrabalak, S. E. Aerosol-Assisted Synthesis of Shape-Controlled CoFe₂O₄: Topotactic versus Direct Melt Crystallization. *Chem. Mater.* **2015**, *27*, 1863–1868.

(25) Fu, J.; Skrabalak, S. E. Aerosol Synthesis of Shape-Controlled Template Particles: A Route to Ta₃N₅ Nanoplates and Octahedra as Photocatalysts. *J. Mater. Chem. A* **2016**, *4*, 8451–8457.

(26) Fu, J.; Skrabalak, S. E. Enhanced Photoactivity from Single-Crystalline SrTaO₂N Nanoplates Synthesized by Topotactic Nitridation. *Angew. Chem., Int. Ed.* **2017**, *56*, 14169–14173.

(27) Boltersdorf, J.; King, N.; Maggard, P. A. Flux-Mediated Crystal Growth of Metal Oxides: Synthetic Tunability of Particle Morphologies, Sizes, and Surface Features for Photocatalysis Research. *CrystEngComm* **2015**, *17*, 2225–2241.

(28) Mehring, M. From Molecules to Bismuth Oxide-Based materials: Potential Homo- and Heterometallic Precursors and Model Compounds. *Coord. Chem. Rev.* **2007**, *251*, 974–1006.

(29) Summers, S. P.; Abboud, K. A.; Farrah, S. R.; Palenik, G. J. Synthesis and Structures of Bismuth(III) Complexes with Nitrilotriacetic Acid, Ethylenediaminetetraacetic Acid, and Diethylenetriaminepentaacetic Acid. *Inorg. Chem.* **1994**, *33*, 88–92.

(30) Briand, G. G.; Burford, N. Bismuth Compounds and Preparations with Biological or Medicinal Relevance. *Chem. Rev.* **1999**, *99*, 2601–2657.

(31) Kiprof, P.; Scherer, W.; Pajdla, L.; Herdtweck, E.; Herrmann, W. A. Bismutlactat: Darstellung und Strukturchemie eines Hydroxycarboxylat-Komplexes. *Chem. Ber.* **1992**, *125*, 43–46.

(32) Munasinghe, H. N.; Suescun, L.; Dhanapala, B. D.; Rabuffetti, F. A. Bimetallic Trifluoroacetates as Precursors to Layered Perovskites A₂MnF₄ (A = K, Rb, and Cs). *Inorg. Chem.* **2020**, *59*, 17268–17275.

(33) Szlag, R. G.; Suescun, L.; Dhanapala, B. D.; Rabuffetti, F. A. Rubidium-Alkaline-Earth Trifluoroacetate Hybrids as Self-Fluorinating Single-Source Precursors to Mixed-Metal Fluorides. *Inorg. Chem.* **2019**, *58*, 3041–3049.

(34) Dhanapala, B. D.; Munasinghe, H. N.; Suescun, L.; Rabuffetti, F. A. Bimetallic Trifluoroacetates as Single-Source Precursors for Alkali-Manganese Fluoroperovskites. *Inorg. Chem.* **2017**, *56*, 13311–13320.

(35) Akiya, N.; Savage, P. E. Roles of Water for Chemical Reactions in High-Temperature Water. *Chem. Rev.* **2002**, *102*, 2725–2750.

(36) Urbansky, E. T. The Fate of the Haloacetates in Drinking Water-Chemical Kinetics in Aqueous Solution. *Chem. Rev.* **2001**, *101*, 3233–3243.

(37) Blandamer, M. J.; Robertson, R. E.; Scott, J. M. W.; Vrieling, A. Evidence for the Incursion of Intermediates in the Hydrolysis of Tertiary, Secondary, and Primary Substrates. *J. Am. Chem. Soc.* **1980**, *102*, 2585–2592.

(38) Bunnett, J. F. Nucleophilic Reactivity. *Annu. Rev. Phys. Chem.* **1963**, *14*, 271–290.

(39) Jencks, W. P. When Is an Intermediate Not an Intermediate? Enforced Mechanisms of General Acid-Base Catalyzed, Carbocation, Carbanion, and Ligand Exchange Reactions. *Acc. Chem. Res.* **1980**, *13*, 161–169.

(40) Hu, C.; Cun, X.; Ruan, S.; Liu, R.; Xiao, W.; Yang, X.; Yang, Y.; Yang, C.; Gao, H. Enzyme-Triggered Size Shrink and Laser-Enhanced NO Release Nanoparticles for Deep Tumor Penetration and Combination Therapy. *Biomaterials* **2018**, *168*, 64–75.

(41) Ziakas, G. N.; Rekka, E. A.; Gavalas, A. M.; Eleftheriou, P. T.; Tsiakitzis, K. C.; Kourounakis, P. N. Nitric Oxide Releasing Derivatives of Tolfenamic Acid with Anti-Inflammatory Activity and Safe Gastrointestinal Profile. *Bioorg. Med. Chem.* **2005**, *13*, 6485–6492.

(42) Kudo, A.; Miseki, Y. Heterogeneous Photocatalyst Materials for Water Splitting. *Chem. Soc. Rev.* **2009**, *38*, 253–278.

(43) Wang, Q.; Domen, K. Particulate Photocatalysts for Light-Driven Water Splitting: Mechanisms, Challenges, and Design Strategies. *Chem. Rev.* **2020**, *120*, 919–985.

(44) Xiong, Y.; Kudas, T. T. Droplet Evaporation and Solute Precipitation During Spray Pyrolysis. *J. Aerosol Sci.* **1993**, *24*, 893–908.

(45) Ganose, A. M.; Cuff, M.; Butler, K. T.; Walsh, A.; Scanlon, D. O. Interplay of Orbital and Relativistic Effects in Bismuth Oxyhalides: BiOF, BiOCl, BiOBr, and BiOI. *Chem. Mater.* **2016**, *28*, 1980–1984.

(46) Bhachu, D. S.; Moniz, S. J. A.; Sathasivam, S.; Scanlon, D. O.; Walsh, A.; Bawaked, S. M.; Mokhtar, M.; Obaid, A. Y.; Parkin, I. P.; Tang, J.; Carmalt, C. J. Bismuth Oxyhalides: Synthesis, Structure and Photoelectrochemical Activity. *Chem. Sci.* **2016**, *7*, 4832–4841.

(47) Li, Z.; Huang, G.; Liu, K.; Tang, X.; Peng, Q.; Huang, J.; Ao, M.; Zhang, G. Hierarchical BiOX (X = Cl, Br, I) Microrods Derived from Bismuth-MOFs: In Situ Synthesis, Photocatalytic Activity and Mechanism. *J. Cleaner Prod.* **2020**, *272*, 122892.

(48) Yang, J.; Wang, D.; Han, H.; Li, C. Roles of Cocatalysts in Photocatalysis and Photoelectrocatalysis. *Acc. Chem. Res.* **2013**, *46*, 1900–1909.

(49) Dong, X.; Zhang, W.; Sun, Y.; Li, J.; Cen, W.; Cui, Z.; Huang, H.; Dong, F. Visible-Light-Induced Charge Transfer Pathway and Photocatalysis Mechanism on Bi Semimetal@Defective BiOBr Hierarchical Microspheres. *J. Catal.* **2018**, *357*, 41–50.

(50) Ye, L.; Deng, Y.; Wang, L.; Xie, H.; Su, F. Bismuth-Based Photocatalysts for Solar Photocatalytic Carbon Dioxide Conversion. *ChemSusChem* **2019**, *12*, 3671–3701.

(51) Shiraiishi, Y.; Hashimoto, M.; Chishiro, K.; Moriyama, K.; Tanaka, S.; Hirai, T. Photocatalytic Dinitrogen Fixation with Water on Bismuth Oxychloride in Chloride Solutions for Solar-to-Chemical Energy Conversion. *J. Am. Chem. Soc.* **2020**, *142*, 7574–7583.